Supplementary Materials

X-ray Diffraction Samples and Measurements

X-ray diffraction analysis of the Rocknest scoop sample is described in (*23*); similar analyses were performed for John Klein and Cumberland. John Klein and Cumberland were the first two drill samples collected by *Curiosity*. All scooped or drilled samples pass through the Collection and Handling for In situ Martian Rock Analysis (CHIMRA) sample collection and processing system (*10*). All powders for X-ray diffraction are processed through a 150-μm sieve before delivering a portion to the CheMin inlet funnel.

The sieved drill powders were placed into sample cells with 6 μm thick Mylar® windows. Mylar® contributes a minor, broad scattering signature in diffraction patterns that is generally "swamped" by diffraction from the loaded sample. In addition, an aluminized light shield also contributes "peaks" to the observed diffraction patterns. Only ~10 mm^3 of material is required to fill the active volume of the sample cell, which is a disc-shaped volume 8 mm in diameter and 175 μm thick. A collimated ~70 μm diameter X-ray beam illuminates the center of the sample cell. A piezoelectric vibration system on each cell pair shakes the material during analysis, causing grains in the cell to pass through the X-ray beam in random orientations.

CheMin measures XRD and XRF data simultaneously using Co radiation in transmission geometry (*11*). The instrument operates in single-photon counting mode so that between each readout the majority of CCD pixels are struck by either a single X-ray photon or by no photons. In this way, the system can determine both the energy of the photons striking the CCD (XRF) and the two-dimensional (2-D) position of each photon (XRD). The energy and positional information of detected photons in each frame are summed over repeated 10-sec measurements into a "minor frame" of 30 min of data (180 frames). The 2-D distribution of Co Kα X-ray intensity represents the XRD pattern of the sample. Circumferential integration of these rings, corrected for arc length, produces a conventional 1-D XRD pattern. For conversion of the 2-D CCD pattern to a 1-D pattern we have used FilmScan© software from Materials Data, Inc.

CheMin generally operates for only a few hours each night, when the CCD can be cooled to its lowest temperature, collecting as many minor frames as possible for the available analysis time, usually five to seven per night. XRD data were acquired over multiple nights for the John Klein and Cumberland drill samples to provide acceptable counting statistics. Total data collection times were 33.9 hr for John Klein and 20.2 hr for Cumberland. The data for individual minor frames and for each night's analysis were examined separately, and there was no evidence of any changes in instrumental parameters as a function of time over the duration of these analyses. Before sample delivery and analysis, the empty cell was analyzed to confirm that it was indeed empty before receiving the sample. The flight instrument was calibrated on the ground before flight using a quartz-beryl standard, and measurement of this standard on Mars showed no changes in instrument geometry or dimensions.

Crystalline Components. All XRD data were first evaluated by comparisons and searches of the International Centre for Diffraction Data (ICDD) Powder Diffraction File using Bruker AXS DIFFRAC.EVA (©2000, Bruker AXS, Karlsruhe, Germany) and MDI Jade© (Materials Data Incorporated, Livermore, CA) software packages, which revealed the presence of plagioclase, forsterite, magnetite, augite, pigeonite, orthopyroxene, akaganeite, bassanite, and anhydrite. John

Klein was the first drill sample analyzed and there was immediate evidence of a phyllosilicate, represented by a broad diffraction peak at 8.5-11° 2θ Co Kα. The comparatively large instrumental peak width for the CheMin instrument (~0.3° 2θ full-width at half-maximum at 25° 2θ) limits our ability to determine accurately the presence of some minor crystalline phases (<2 wt. %). The data were analyzed further via Rietveld methods, using Topas (©2000, Bruker AXS, Karlsruhe, Germany). We used the fundamental-parameters approach within Topas, along with additional convolutions, to model the experimental profiles. We also used an emission spectrum including Co Kα with a refinable Co Kβ component. The Rietveld method involves constructing a model consisting of the crystal structures of all component phases, and the differences between the observed and simulated diffraction patterns are minimized by varying components of the model, including scale factors (related to phase abundance), unit-cell parameters, and crystallite-size and strain broadening parameters for each phase. Atomic positions and site occupancies were generally not varied, although octahedral site occupancies were varied for forsteritic olivine, augite, and pigeonite, and Na-Ca occupancies were varied for the plagioclase component. This method thus provides information on all well-ordered phases (*i.e.*, crystalline), but it is not directly applicable to disordered phases such as clay minerals or amorphous components.

Clay Mineral and Amorphous-component Abundances. Neither smectites nor X-ray amorphous samples are amenable to Rietveld analysis. Instead, the FULLPAT full-pattern fitting method was used (*22*). FULLPAT operates on the principle that diffraction and scattering patterns for all phases in a sample are additive. By fitting full diffraction patterns, including the background, which contains important information on sample composition and matrix effects, explicit analysis of amorphous or partially ordered materials can be accomplished if the amorphous/disordered phases are included in the analyses as distinct phases. Thus, FULLPAT allows direct analysis of the abundance of clay minerals and amorphous components, rather than determining them as the difference from 100% in an internal-standard quantitative analysis. Like all full-pattern fitting methods, accurate analysis requires representative standards or structure models. A large variety of pure mineral standards, disordered materials (allophanes, ferrihydrite, aluminosilicate gels), and a synthetic glass of Gusev basaltic composition were measured. Each of these was run as a pure phase and was also mixed with a beryl standard in 50:50 wt. ratio to determine a Reference Intensity Ratio (RIR) for subsequent use in FULLPAT. All standard data were measured on a CheMin IV instrument at the NASA Johnson Space Center; the CheMin IV instrument geometry is very similar to the instrument on MSL and is considered a good proxy for the flight instrument. Peak areas for each phase were compared against the intensity of the beryl 100 peak, and the measured beryl RIR of 1.70 relative to corundum (measured on a laboratory instrument) was used to convert the RIR(beryl) to the conventional RIR(corundum) value. During FULLPAT analysis, the intensity of each standard pattern was normalized to the intensity of a pure pattern of corundum used as datum. Thus, using the corundum datum 113 reflection intensity and the measured RIR for each standard phase, the pattern of each disordered phase could be normalized to the appropriate overall intensity based on its measured intensity area used for the RIR determination.

Because few standard data for pure phases have been measured on the CheMin flight instrument, an alternate method for calculating standard data representative of the MSL CheMin instrument was also employed. This process involved first determining instrumental peak shapes and widths as a function of 2θ using the beryl standard measured on the MSL instrument. We

then calculated diffraction patterns for each standard using the appropriate crystal structure information and the instrumental profiles determined above for Co Kα radiation. The final step in calculation of standard data for FULLPAT is to normalize the intensity of the calculated pattern to the corundum datum pattern using the calculated RIR as outlined above. The scaled measured and calculated library patterns, for both ordered and amorphous phases, were then used with FULLPAT.

Estimating Compositions and Abundances of Clay Minerals and Amorphous Components from XRD and APXS data.

The relative proportions of crystalline and amorphous plus smectite components and their respective bulk compositions were estimated by combining the APXS chemical compositions of the mudstone samples, and the chemical composition of crystalline components including Fe oxidation state (from stoichiometry or XRD unit-cell parameters) weighted by their CheMin XRD abundance (phases from plagioclase to pyrrhotite in Table 1 in this paper). To estimate the chemical composition of the amorphous material relative to that of the total amorphous plus smectite component, the chemical compositions (H_2O/OH-free basis) of two saponites were assumed for the trioctahedral smectite: griffithite and Clay Minerals Society saponite SapCa-1. Among the clay minerals analyzed in the laboratory, griffithite has an 02*l* diffraction band similar to the smectite component of both John Klein and Cumberland. The proportion of each smectite, calculated by increasing the smectite concentration until the MgO concentration in the amorphous component was ~0 wt.%, is an upper limit for its concentration.

Table S-1. Chemical composition of John Klein drill fines from APXS and CheMin measurements, calculated chemical compositions of crystalline and combined amorphous and smectite components, and calculated chemical compositions of amorphous components assuming griffithite and saponite SapCa-1 as trioctahedral smectites.

		APXS	XRD	Smectite+	Griffithite Model[e]		SapCa-1 Model[f]	
(wt.%)	APXS[a]	+CHMN[b]	Crystalline[c]	Amorphous[d]	Griffithite	Amorphous	SapCa-1	Amorphous
SiO_2	42.07	42.03	42.65	41.76	49.71	32.94	57.60	30.10
TiO_2	0.97	0.97	-0.02	1.41	-0.01	2.98	0.56	2.03
Al_2O_3	8.67	8.66	12.48	6.97	9.52	4.14	4.11	9.08
Cr_2O_3	0.42	0.42	-0.01	0.61	-0.01	1.30	-0.02	1.07
$FeO+Fe_2O_3$	19.86	13.51	-0.23	19.59	16.48	23.04	0.74	33.46
Fe-Cryst	0.00	0.47	1.51	0.00	0.00	0.01	0.00	0.01
FeO-Cryst	0.00	3.24	10.53	0.00	0.00	0.00	0.00	0.00
Fe_2O_3-Cryst	0.00	2.06	6.71	0.00	0.00	0.00	0.00	0.00
Fe_2O_3-npOx	0.00	0.58	1.87	0.00	0.00	0.00	0.00	0.00
MnO	0.27	0.27	0.00	0.39	0.07	0.75	0.03	0.66
MgO	9.06	9.05	4.88	10.90	20.66	0.07	25.70	0.01
CaO	7.76	7.75	9.47	6.99	2.83	11.61	7.72	6.46
Na_2O	3.01	2.90	2.98	2.86	0.05	5.98	1.75	3.68
Na-Cryst	0.00	0.04	0.13	0.00	0.00	0.00	0.00	0.00
K_2O	0.57	0.57	0.30	0.69	0.01	1.44	0.87	0.56
P_2O_5	0.93	0.93	-0.02	1.35	-0.02	2.87	0.09	2.28
SO_3	5.61	3.83	1.07	5.05	-0.09	10.76	0.07	8.72
S-Cryst	0.00	0.33	1.07	0.00	0.00	0.01	0.00	0.01
SO_3-Cryst	0.00	0.95	3.10	0.00	0.00	-0.01	0.00	-0.01
Cl	0.56	0.53	0.33	0.62	-0.01	1.31	-0.02	1.08
H_2O-Cyst	0.00	0.12	0.40	0.00	0.00	-0.01	0.00	0.00
Sum	99.76	99.20	99.20	99.20	99.19	99.19	99.20	99.19
Relative to Whole Sample			30.7	69.3	36.4	32.8	29.4	39.9

[a]Composition of drill fines. [b]Composition of drill fines modified according to chemical composition of XRD crystalline phases (excluding smectite). [c]Composition of XRD crystalline component calculated from compositions of individual crystalline components and their relative proportions from Table 1. [d]Composition of amorphous plus smectite component. Cr_2O_3, MnO, and P_2O_5 were modeled with the amorphous component. [e]Composition of griffithite (H_2O/OH-free basis) and the amorphous phase calculated assuming griffithite is the smectite and MgO ~0 wt.% in the amorphous phase. [f]Composition of SapCa-1 (H_2O/OH-free basis) and the amorphous phase calculated assuming SapCa-1 is the smectite and MgO ~0 wt.% in the amorphous phase.

Table S-2. Chemical composition of Cumberland drill fines from APXS and CheMin measurements, calculated chemical compositions of crystalline and combined amorphous and smectite components, and calculated chemical compositions of amorphous components assuming griffithite and saponite SapCa-1 as trioctahedral smectites.

		APXS	XRD	Smectite+	Griffithite Model[e]		SapCa-1 Model[f]	
(wt.%)	APXS[a]	+CHMN[b]	Crystalline[c]	Amorphous[d]	Griffithite	Amorphous	SapCa-1	Amorphous
SiO_2	43.02	43.33	43.72	43.15	49.71	34.98	57.59	31.54
TiO_2	0.97	0.98	0.57	1.16	-0.01	2.62	0.57	1.64
Al_2O_3	8.57	8.63	12.38	6.96	9.53	3.75	4.11	9.25
Cr_2O_3	0.43	0.43	-0.01	0.63	-0.01	1.43	-0.02	1.15
$FeO+Fe_2O_3$	22.35	15.27	-0.25	22.21	16.43	29.39	0.66	39.54
Fe-Cryst	0.00	0.38	1.23	0.00	0.00	0.00	0.00	0.00
FeO-Cryst	0.00	3.63	11.74	0.00	0.00	0.00	0.00	0.00
Fe_2O_3-Cryst	0.00	2.37	7.65	0.01	0.00	0.02	0.00	0.01
Fe_2O_3-npOx	0.00	0.86	2.79	0.00	0.00	0.00	0.00	0.00
MnO	0.27	0.27	0.00	0.40	0.07	0.80	0.03	0.69
MgO	9.41	9.48	5.00	11.48	20.66	0.02	25.70	0.03
CaO	6.29	6.34	7.91	5.63	2.86	9.09	7.75	3.92
Na_2O	2.98	2.87	2.86	2.97	0.05	6.60	1.74	3.95
Na-Cryst	0.00	0.05	0.08	0.00	0.00	0.00	0.00	0.00
K_2O	0.50	0.50	0.39	0.55	0.01	1.23	0.88	0.30
P_2O_5	0.95	0.96	-0.02	1.39	-0.02	3.16	0.08	2.44
SO_3	2.57	1.61	0.73	2.00	-0.04	4.55	0.15	3.50
S-Cryst	0.00	0.28	0.74	0.07	0.00	0.17	0.00	0.13
SO_3-Cryst	0.00	0.28	0.91	0.00	0.00	-0.01	0.00	-0.01
Cl	1.39	0.53	0.32	0.63	-0.01	1.43	-0.02	1.15
H_2O-Cyst	0.00	0.15	0.49	0.00	0.00	0.00	0.00	0.00
Sum	99.70	99.20	99.24	99.24	99.23	99.23	99.23	99.23
Relative to Whole Sample			30.9	69.1	38.4	30.7	30.8	38.3

[a]Composition of drill fines. [b]Composition of drill fines modified according to chemical composition of XRD crystalline phases (excluding smectite). [c]Composition of XRD crystalline component calculated from compositions of individual crystalline components and their relative proportions from Table 1. [d]Composition of amorphous plus smectite component. Cr_2O_3, MnO, and P_2O_5 are modeled with the amorphous component. [e]Composition of griffithite (H_2O/OH-free basis) and the amorphous phase calculated assuming griffithite is the smectite and MgO ~0 wt.% in the amorphous phase. [f]Composition of SapCa-1 (H_2O/OH-free basis) and the amorphous phase calculated assuming SapCa-1 is the smectite and MgO ~0 wt.% in the amorphous phase.

Mastcam Hydration Signatures

The Mastcam instrument is a pair of CCD cameras with fixed focal lengths (34-mm and 100-mm) mounted roughly 2-m above the surface on the rover's mast (*14*). Each camera obtains images through a Bayer pattern of RGB filters and telecentric microlenses bonded onto the CCD and an 8-position narrowband filter wheel that provides the ability to obtain spectra in 12 unique wavelengths (*41*). These multispectral observations have been calibrated to radiance (*I*) using pre-flight calibration coefficients, to radiance factor (*I/F*, where πF is the solar irradiance at the top of the Martian atmosphere at the time of the observation) using associated observations of the Mastcam calibration target, and to relative reflectance (*R**) by dividing *I/F* by the cosine of

the solar incidence angle (a similar procedure was used to calibrate Mars Exploration Rover (MER) Pancam images to *I/F* and *R**; (*66, 67*)).

Mastcam's longest wavelength filters have some sensitivity to hydrated and/or hydroxylated minerals (*27*). Specifically, the 1013 nm near-IR filters (referred to as filters L6 and R6 (*41*)) can detect an absorption due to the $2\nu_1 + \nu_3$ H_2O combination band and/or the 3ν OH overtone when this band minimum occurs longward of roughly 980 nm (*e.g.*, as in water ice, some carbonates, and hydrated sulfates). This narrow hydration band leads to a Mastcam spectral profile that is "flat" in the near-IR, with a sharp downturn at the longest Mastcam wavelength (Fig. 4C) that can be used as a "hydration signature." This profile is distinguishable from spectra of iron-bearing minerals with broad absorptions near 1000-nm, which have an overall negative spectral slope in the near-IR.

The Mastcam hydration signature can be used to remotely identify and map candidate hydrated surface materials in Mastcam near-IR filter images based on the technique developed for the MER Pancam instruments (*16, 68*) and applied to images acquired along the Spirit (*16, 69*) and Opportunity (*38, 70*) traverses. Mastcam spectra exhibiting a hydration signature are defined as those with a spectral slope ($\Delta R^*/\Delta\lambda$) in calibrated *R** data from 937 to 1013 nm less than -4.0×10^{-4} nm^{-1} and a nearly-flat *R** spectral profile between 805 and 937 nm (with absolute slope values less than 2.0×10^{-4} nm^{-1}). Slope thresholds were modified slightly from those used for the Pancam hydration signature (*16*) in order to minimize noise in the Mastcam hydration maps.

It is important to note that the absence of a hydration signature in Mastcam data does not necessarily indicate an absence of hydrated minerals; in the spectra of many H_2O and/or OH bearing minerals, including phyllosilicates such as saponite (Fig. 4C), the hydration band is centered closer to 950 nm and cannot be detected by Mastcam's longest wavelength filter. Of the various hydration states of Ca-sulfate (gypsum, bassanite and anhydrite), only gypsum ($CaSO_4 \cdot 2H_2O$) is detectable to Mastcam (and also to MER Pancam (*38*)). Anhydrite ($CaSO_4$) lacks a hydration band, and the weak hydration band in bassanite ($CaSO_4 \cdot 0.5H_2O$) is centered near 950 nm (Fig. 4C).

Mapping of Light-toned Veins and Nodules in Borehole Walls

Light-toned veins and nodules are visible in both the John Klein and Cumberland borehole walls. Analyses by LIBS and APXS indicate that these late-diagenetic features are associated with Ca-sulfate; in contrast the mudstone matrix is relatively sulfate-poor (*8, 19*). Sulfate minerals detected by CheMin in the borehole samples include anhydrite and bassanite. An initial ChemCam RMI image taken to support localization of the LIBS analysis spots also showed a striking distribution of veins and nodules in the John Klein drill hole. Subsequently, to better understand the distribution of late-diagenetic veins and nodules, several off-axis images of both boreholes were taken using the Mars Hand Lens Imager (MAHLI) to get relatively complete coverage of the borehole walls to the full visible depth. Some images were acquired at night using MAHLI white light LED illumination. The images were processed to compare the light-toned vein and nodule abundances between John Klein and Cumberland, and to compare sulfate mineral abundances determined by CheMin with mapped abundances of light-toned fillings.

Drill hole depth and wall visibility - Both the John Klein and Cumberland holes were drilled to a depth of about 6.5 cm. Autofocused MAHLI image sub-frames covering only the floor of each hole—acquired shortly after drilling was completed on the same sol that the rock was drilled—provided a measure of the distance between the camera lens and the bottom of the hole. Similar autofocused sub-frames acquired outside the hole permitted subtraction of one from the other to estimate hole depth. In both cases, the hole was measured to be about 3.2 ± 0.3 cm deep. While the drill penetrated to 6.5 cm, drill cuttings/debris filled the lower half of each after the drill bit was withdrawn. These ranges, relative to the MAHLI lens, were estimated from its focus motor count position (m), which, when the dust cover is open and the range is between 2.1 and 210 cm, relates to range (r, in cm) between lens and target by $r = ((0.576786m^{-1}) + (-11.8479) + (2.80153\times10^{-3}m) + (-2.266488\times10^{-7}m^2) + (6.26666\times10^{-12}m^3))^{-1}$. Thus, for the drill hole wall analysis presented here, only half of the depth and half of the surface area of each wall was observed.

Processing - Of the focus stack images acquired at each drill hole, those that were in best focus on the drill hole walls were chosen to accurately represent the entire surface area of the drill hole. Both the John Klein and Cumberland drill holes have MAHLI images from four map directions (approximately S, W, N, E). Some of the MAHLI nighttime LED-illuminated images show more detail of the vein material than do the day, solar-illuminated, images, such as the W, N and E images for Cumberland. Images with the least compression and best focus and contrast were selected and each was cropped in Adobe Photoshop© to 1903 pixels wide and 1847 pixels high, or 6.343 inches wide and 6.157 inches high, at 300 dpi. The width is slightly larger than the height due to the ellipsoid shape of the drill hole as viewed from off-axis angles. A master image was created to hold all the images. The master image is 3805 pixels wide and 3693 pixels high, or 25.543 inches wide and 24.597 inches high, at 300 dpi. Drill hole images were aligned from left to right in order S, W, N, E with the long axis of the drill hole ellipse oriented left-right. Some of the images were tilted and/or had different image scales. In order to correct this, one drill hole image was selected to be the template orientation (long axis left-right) and size. A new layer was created so that an ellipse template could be created to correctly align and size the other images. In the new layer the elliptical marquee tool was used to trace out an ellipse that exactly fit the image that was selected as the base image. That layer was copied and pasted to cover all four images. Each drill hole image was then aligned with the transformation tool to best fit the

ellipse template and the opacity of the ellipse templates was adjusted to 50%. The drill hole ellipse template was used as the surface area marker for mapping. Some of the images overlapped, in which case the image with the best representation of the vein was used.

Easily identifiable marks in the images were used to end one image and start another, so that the entire surface was represented with no overlap. The ellipses were then cut with the polygonal lasso tool to represent the mapping area. The regular lasso tool was used to remove from the image any drill cuttings or debris visible on the bottom of the drill hole. All four images were then converted to greyscale (second row of images in Figs. S-1 and S-2). The bottom row of images was processed to enhance contrast to better show the veins. Next, the previously created surface area marker layers were copied and placed over the bottom row of high contrast images. These were used to cut out un-mapped areas of the drill holes. Each drill-hole image was cut and copied into a new layer. Surface-area marker layers were processed one at a time by using the color range tool to select light-toned vein material. The vein representation was increased to include different shades by selecting additional vein colors until a good representation of the veins was obtained. The selected area was added or removed with the lasso tool. After this was done, the actual drill hole image was deselected and the surface area marker was selected to create a simple representation of the vein in the mapping area.

The vein-to-total surface area percentage was derived from this final representation. The surface area marker was selected with the magic wand tool and the expanded view of the histogram window. With the full area minus the vein area, the histogram window was refreshed to give a pixel amount. This was repeated for every surface area marker and the results were used to calculate vein/(vein + surface minus vein) = percent vein per total surface area.

Results - The surface area of vein exposure in Cumberland is ~1.7%, very similar to the total sulfate mineral abundance of 1.5% (bassanite plus anhydrite, based on the abundances in Table 1). The surface area of vein exposure in John Klein is ~5.2%, compared with a total sulfate mineral abundance of 3.6% (bassanite plus anhydrite, based on the abundances in Table 1). The apparent excess of mapped vein area compared to sulfate mineral abundance, notably in the John Klein borehole and sample, could be attributed to several factors, including the generally low grain densities of the Ca-sulfates (ρ ~2.73 for bassanite to ~2.97 for anhydrite, slightly more than andesine at ~2.67 but less than the pyroxenes at ~3.3-3.7 and much less than magnetite at ~5.1). However, the greater contributors to the difference are likely to be the inability to map the full borehole depth because of fill (the upper ~1.5 cm of the borehole does not make it into the sample processing system (*10*)), the unknown bulk densities of both the veins and the matrix, the errors in image analysis and quantitative crystalline XRD, and the errors in estimating abundances of the amorphous and clay mineral components from XRD data. Nevertheless, the mapped vein areas in both boreholes are sufficient to account for all of the sulfates detected by XRD.

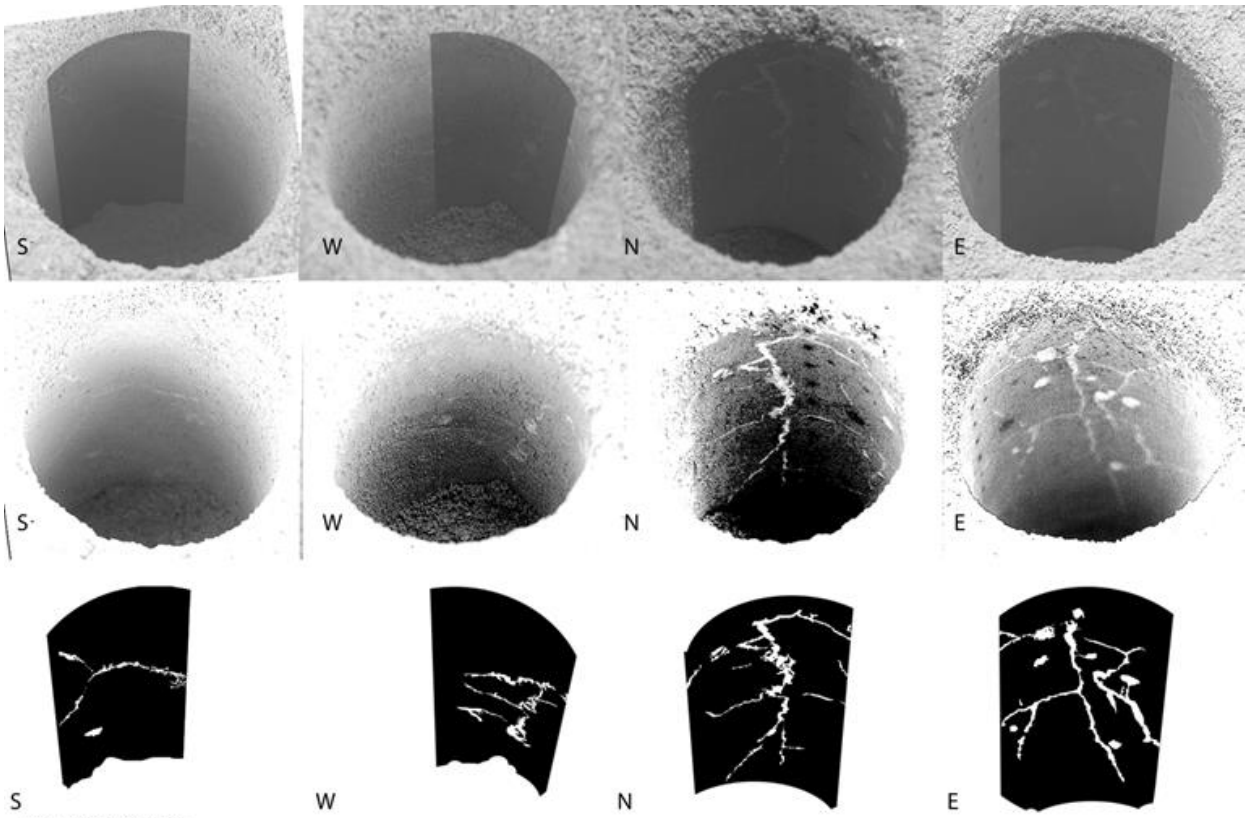

Fig. S-1: Analysis of veins in the John Klein borehole wall. Upper row shows primary images in grayscale with sectors (black) selected for mapping from each MAHLI image (MAHLI images collected on sol 270). Second row from top shows contrast-stretched images (note dark LIBS laser spots in the north image). Bottom row shows images processed to enhance the pixel representation of vein and nodule abundances for quantitative analysis; total vein and nodule area is 5.18% of the borehole wall.

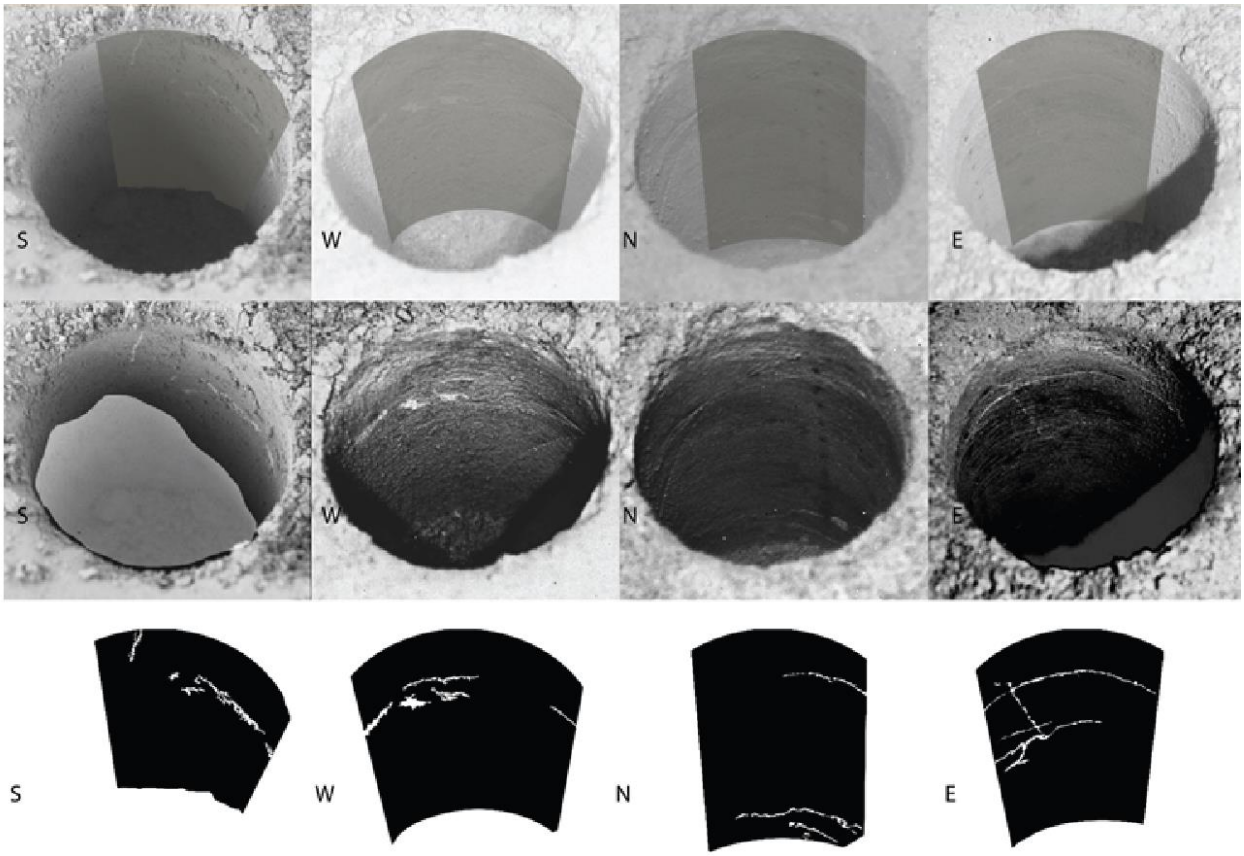

Fig. S-2. Analysis of veins in the Cumberland borehole wall. Upper row shows primary images in grayscale with sectors (black) selected for mapping from each MAHLI image (MAHLI images collected on sol 279). Second row from top shows contrast-stretched images. Bottom row shows images processed for pixel representation of vein and nodule abundances; vein and nodule area is 1.74% of the borehole wall.

Mars Science Laboratory Science Team:

Achilles, Cherie	Jacobs Technology (at NASA JSC)
Agard, Christophe	CNES (Centre National d'Etudes Spatiales)
Alves Verdasca, José Alexandre	CAB (Centro de Astrobiología)
Anderson, Robert	NASA JPL
Anderson, Ryan	USGS Flagstaff
Archer, Doug	NASA Postdoc Program (at NASA JSC)
Armiens-Aparicio, Carlos	CAB (Centro de Astrobiología)
Arvidson, Ray	WUSTL (Washington University in St. Louis)
Atlaskin, Evgeny	FMI (Finnish Meteorological Institute) and University of Helsinki
Atreya, Sushil	University of Michigan Ann Arbor
Aubrey, Andrew	NASA JPL
Baker, Burt	MSSS (Malin Space Science Systems)
Baker, Michael	Caltech
Balic-Zunic, Tonci	University of Copenhagen
Baratoux, David	IRAP (Institut de Recherche en Astrophysique et Planetologie)
Baroukh, Julien	CNES (Centre National d'Etudes Spatiales)
Barraclough, Bruce	PSI (Planetary Science Institute)
Bean, Keri	Texas A&M
Beegle, Luther	NASA JPL
Behar, Alberto	NASA JPL
Bell, James	ASU (Arizona State University)
Bender, Steve	PSI (Planetary Science Institute)
Benna, Mehdi	University of Maryland Baltimore County (at NASA GSFC)
Bentz, Jennifer	University of Saskatchewan

Berger, Gilles	IRAP (Institut de Recherche en Astrophysique et Planetologie)
Berger, Jeff	University of New Mexico (Western Univ. May 1)
Berman, Daniel	PSI (Planetary Science Institute)
Bish, David	Indiana University Bloomington
Blake, David F.	NASA Ames
Blanco Avalos, Juan J.	Universidad de Alcalá de Henares
Blaney, Diana	NASA JPL
Blank, Jen	BAER (at NASA Ames)
Blau, Hannah	University of Massachusetts
Bleacher, Lora	USRA-LPI (at NASA GSFC)
Boehm, Eckart	University of Kiel
Botta, Oliver	Swiss Space Office
Böttcher, Stephan	University of Kiel
Boucher, Thomas	University of Massachusetts
Bower, Hannah	University of Maryland College Park
Boyd, Nick	University of Guelph
Boynton, Bill	University of Arizona
Breves, Elly	Mount Holyoke College
Bridges, John	University of Leicester
Bridges, Nathan	APL (Johns Hopkins University Applied Physics Laboratory)
Brinckerhoff, William	NASA GSFC
Brinza, David	NASA JPL
Bristow, Thomas	NASA Postdoc Program (at NASA Ames)
Brunet, Claude	CSA (Canadian Space Agency)

Brunner, Anna	University of Maryland College Park (at GSFC)
Brunner, Will	inXitu
Buch, Arnaud	LGPM, Ecole Centrale Paris (Laboratoire Génie des Procédés et Matériaux)
Bullock, Mark	SwRI (Southwest Research Institute)
Burmeister, Sönke	University of Kiel
Cabane, Michel	LATMOS (Laboratoire Atmosphères, Milieux, Observations Spatiales)
Calef, Fred	NASA JPL
Cameron, James	Lightstorm Entertainment Inc.
Campbell, John "Iain"	University of Guelph
Cantor, Bruce	MSSS (Malin Space Science Systems)
Caplinger, Michael	MSSS (Malin Space Science Systems)
Caride Rodríguez, Javier	CAB (Centro de Astrobiología)
Carmosino, Marco	University of Massachusetts
Carrasco Blázquez, Isaías	CAB (Centro de Astrobiología)
Charpentier, Antoine	ATOS Origin
Chipera, Steve	Chesapeake Energy
Choi, David	NASA Postdoc Program (at NASA GSFC)
Clark, Benton	SSI (Space Science Institute)
Clegg, Sam	LANL (Los Alamos National Lab)
Cleghorn, Timothy	NASA JSC
Cloutis, Ed	University of Winnipeg
Cody, George	Carnegie Institution of Washington
Coll, Patrice	LISA (Laboratoire Interuniversitaire des Systèmes

	Atmosphériques), Université Paris
Conrad, Pamela	NASA GSFC
Coscia, David	LATMOS (Laboratoire Atmosphères, Milieux, Observations Spatiales)
Cousin, Agnès	LANL (Los Alamos National Lab)
Cremers, David	ARA (Applied Research Associates, Inc.)
Crisp, Joy	NASA JPL
Cros, Alain	IRAP (Institut de Recherche en Astrophysique et Planetologie)
Cucinotta, Frank	NASA JSC
d'Uston, Claude	IRAP (Institut de Recherche en Astrophysique et Planetologie)
Davis, Scott	MSSS (Malin Space Science Systems)
Day, Mackenzie "Kenzie"	University of Texas at Austin
de la Torre Juarez, Manuel	NASA JPL
DeFlores, Lauren	NASA JPL
DeLapp, Dorothea	LANL (Los Alamos National Lab)
DeMarines, Julia	Denver Museum of Nature & Science
DesMarais, David	NASA Ames
Dietrich, William	University of California Berkeley
Dingler, Robert	LANL (Los Alamos National Lab)
Donny, Christophe	CNES (Centre National d'Etudes Spatiales)
Downs, Bob	University of Arizona
Drake, Darrell	retired
Dromart, Gilles	LGL-TPE (Laboratoire de Géologié de Lyon : Terre, Planète, Environnement)
Dupont, Audrey	CS Systemes d'Information

Duston, Brian	MSSS (Malin Space Science Systems)
Dworkin, Jason	NASA GSFC
Dyar, M. Darby	Mount Holyoke College
Edgar, Lauren	ASU (Arizona State University)
Edgett, Kenneth	MSSS (Malin Space Science Systems)
Edwards, Christopher	Caltech
Edwards, Laurence	NASA Ames
Ehlmann, Bethany	Caltech
Ehresmann, Bent	SwRI (Southwest Research Institute)
Eigenbrode, Jen	NASA GSFC
Elliott, Beverley	University of New Brunswick
Elliott, Harvey	University of Michigan Ann Arbor
Ewing, Ryan	University of Alabama
Fabre, Cécile	G2R (Géologié et Gestion des Ressources Minérales et Energétique)
Fairén, Alberto	Cornell University
Farley, Ken	Caltech
Farmer, Jack	ASU (Arizona State University)
Fassett, Caleb	Mount Holyoke College
Favot, Laurent	Capgemini France
Fay, Donald	MSSS (Malin Space Science Systems)
Fedosov, Fedor	Space Research Institute
Feldman, Jason	NASA JPL
Feldman, Sabrina	NASA JPL
Fisk, Marty	Oregon State University

Fitzgibbon, Mike	University of Arizona
Flesch, Greg	NASA JPL
Floyd, Melissa	NASA GSFC
Flückiger, Lorenzo	Carnegie Mellon University (at NASA Ames)
Forni, Olivier	IRAP (Institut de Recherche en Astrophysique et Planetologie)
Fraeman, Abby	WUSTL (Washington University in St. Louis)
Francis, Raymond	University of Western Ontario
François, Pascaline	LISA (Laboratoire Interuniversitaire des Systèmes Atmosphériques), Université Paris
Franz, Heather	University of Maryland Baltimore County (at NASA GSFC)
Freissinet, Caroline	NASA Postdoc Program (at NASA GSFC)
French, Katherine Louise	MIT
Frydenvang, Jens	University of Copenhagen
Gaboriaud, Alain	CNES (Centre National d'Etudes Spatiales)
Gailhanou, Marc	CNRS (Centre National de la Recherche Scientifique)
Garvin, James	NASA GSFC
Gasnault, Olivier	IRAP (Institut de Recherche en Astrophysique et Planetologie)
Geffroy, Claude	IC2MP (Institut de Chimie des Milieux et Matériaux de Poitiers)
Gellert, Ralf	University of Guelph
Genzer, Maria	FMI (Finnish Meteorological Institute)
Glavin, Daniel	NASA GSFC
Godber, Austin	ASU (Arizona State University)
Goesmann, Fred	Max Planck Institute for Solar System Research
Goetz, Walter	Max Planck Institute for Solar System Research
Golovin, Dmitry	Space Research Institute

Gómez Gómez, Felipe	Centro de Astrobiología
Gómez-Elvira, Javier	Centro de Astrobiología
Gondet, Brigitte	IAS (Institut d'Astrophysique Spatiale)
Gordon, Suzanne	University of New Mexico
Gorevan, Stephen	Honeybee Robotics
Grant, John	Smithsonian Institution
Griffes, Jennifer	Caltech
Grinspoon, David	Denver Museum of Nature & Science
Grotzinger, John	Caltech
Guillemot, Philippe	CNES (Centre National d'Etudes Spatiales)
Guo, Jingnan	SwRI (Southwest Research Institute)
Gupta, Sanjeev	Imperial College
Guzewich, Scott	NASA Postdoc Program (at NASA GSFC)
Haberle, Robert	NASA Ames
Halleaux, Douglas	University of Michigan Ann Arbor
Hallet, Bernard	University of Washington Seattle
Hamilton, Vicky	(SwRI) Southwest Research Institute
Hardgrove, Craig	MSSS (Malin Space Science Systems)
Harker, David	MSSS (Malin Space Science Systems)
Harpold, Daniel	NASA GSFC
Harri, Ari-Matti	FMI (Finnish Meteorological Institute)
Harshman, Karl	University of Arizona
Hassler, Donald	SwRI (Southwest Research Institute)
Haukka, Harri	FMI (Finnish Meteorological Institute)

Hayes, Alex	Cornell University
Herkenhoff, Ken	USGS Flagstaff
Herrera, Paul	MSSS (Malin Space Science Systems)
Hettrich, Sebastian	CAB (Centro de Astrobiología)
Heydari, Ezat	Jackson State University
Hipkin, Victoria	CSA (Canadian Space Agency)
Hoehler, Tori	NASA Ames
Hollingsworth, Jeff	NASA Ames
Hudgins, Judy	Salish Kootenai College
Huntress, Wesley	Retired
Hurowitz, Joel	NASA JPL
Hviid, Stubbe	Max Planck Institute for Solar System Research
Iagnemma, Karl	MIT
Indyk, Steve	Honeybee Robotics
Israël, Guy	CNRS and LATMOS
Jackson, Ryan	LANL (Los Alamos National Lab)
Jacob, Samantha	University of Hawai'i at Manoa
Jakosky, Bruce	University of Colorado Boulder
Jensen, Elsa	MSSS (Malin Space Science Systems)
Jensen, Jaqueline Kløvgaard	University of Copenhagen
Johnson, Jeffrey	APL (Johns Hopkins University Applied Physics Laboratory)
Johnson, Micah	Microtel (at NASA GSFC)
Johnstone, Steve	LANL (Los Alamos National Lab)
Jones, Andrea	USRA-LPI (at NASA GSFC)

Jones, John	NASA JSC
Joseph, Jonathan	Cornell University
Jun, Insoo	NASA JPL
Kah, Linda	University of Tennessee Knoxville
Kahanpää, Henrik	FMI (Finnish Meteorological Institute)
Kahre, Melinda	NASA Ames
Karpushkina, Natalya	Space Research Institute
Kasprzak, Wayne	NASA GSFC
Kauhanen, Janne	FMI (Finnish Meteorological Institute)
Keely, Leslie	NASA Ames
Kemppinen, Osku	FMI (Finnish Meteorological Institute)
Keymeulen, Didier	NASA JPL
Kim, Myung-Hee	USRA (at NASA JSC)
Kinch, Kjartan	University of Copenhagen
King, Penny	ANU (Australian National University)
Kirkland, Laurel	LPI (Lunar and Planetary Institute)
Kocurek, Gary	University of Texas at Austin
Koefoed, Asmus	University of Copenhagen
Köhler, Jan	University of Kiel
Kortmann, Onno	University of California Berkeley
Kozyrev, Alexander	Space Research Institute
Krezoski, Jill	MSSS (Malin Space Science Systems)
Krysak, Daniel	MSSS (Malin Space Science Systems)
Kuzmin, Ruslan	Space Research Institute and Vernadsky Institute

Lacour, Jean Luc	CEA (Commissariat à l'Énergie Atomique et aux Énergies Alternatives)
Lafaille, Vivian	CNES (Centre National d'Etudes Spatiales)
Langevin, Yves	IAS (Institut d'Astrophysique Spatiale)
Lanza, Nina	LANL (Los Alamos National Lab)
Lasue, Jeremie	IRAP (Institut de Recherche en Astrophysique et Planetologie)
Le Mouélic, Stéphane	LPGN (Laboratoire de Planétologie et Géodynamique de Nantes)
Lee, Ella Mae	USGS Flagstaff
Lee, Qiu-Mei	IRAP (Institut de Recherche en Astrophysique et Planetologie)
Lees, David	Carnegie Mellon University (at NASA Ames)
Lefavor, Matthew	Microtel (at NASA GSFC)
Lemmon, Mark	Texas A&M
Lepinette Malvitte, Alain	CAB (Centro de Astrobiología)
Leshin, Laurie	RPI (Rensselaer Polytechnic Institute)
Léveillé, Richard	CSA (Canadian Space Agency)
Lewin-Carpintier, Éric	ISTerre (Institut des Sciences de la Terre)
Lewis, Kevin	Princeton University
Li, Shuai	Brown University
Lipkaman, Leslie	MSSS (Malin Space Science Systems)
Little, Cynthia	LANL (Los Alamos National Lab)
Litvak, Maxim	Space Research Institute
Lorigny, Eric	CNES (Centre National d'Etudes Spatiales)
Lugmair, Guenter	UCSD (University of California San Diego)
Lundberg, Angela	Delaware State University
Lyness, Eric	Microtel (at NASA GSFC)

Madsen, Morten	University of Copenhagen
Mahaffy, Paul	NASA GSFC
Maki, Justin	NASA JPL
Malakhov, Alexey	Space Research Institute
Malespin, Charles	USRA (at NASA GSFC)
Malin, Michael	MSSS (Malin Space Science Systems)
Mangold, Nicolas	LPGN (Laboratoire de Planétologie et Géodynamique de Nantes)
Manhes, Gérard	Retired
Manning, Heidi	Concordia College
Marchand, Geneviève	CSA (Canadian Space Agency)
Marín Jiménez, Mercedes	CAB (Centro de Astrobiología)
Martín García, César	University of Kiel
Martin, Dave	NASA GSFC
Martin, Mildred	Catholic University of America (at NASA GSFC)
Martínez-Frías, Jesús	Centro de Astrobiología
Martín-Soler, Javier	CAB (Centro de Astrobiología)
Martín-Torres, F. Javier	Centro de Astrobiología
Mauchien, Patrick	CEA (Commissariat à l'Énergie Atomique et aux Énergies Alternatives)
Maurice, Sylvestre	IRAP (Institut de Recherche en Astrophysique et Planetologie)
McAdam, Amy	NASA GSFC
McCartney, Elaina	MSSS (Malin Space Science Systems)
McConnochie, Timothy	University of Maryland (at NASA GSFC)
McCullough, Emily	University of Western Ontario
McEwan, Ian	Ashima Research

McKay, Christopher	NASA Ames
McLennan, Scott	SUNY Stony Brook
McNair, Sean	MSSS (Malin Space Science Systems)
Melikechi, Noureddine	Delaware State University
Meslin, Pierre-Yves	IRAP (Institut de Recherche en Astrophysique et Planetologie)
Meyer, Michael	NASA Headquarters
Mezzacappa, Alissa	Delaware State University
Miller, Hayden	Caltech
Miller, Kristen	MIT
Milliken, Ralph	Brown University
Ming, Douglas	NASA JSC
Minitti, Michelle	ASU (Arizona State University)
Mischna, Michael	NASA JPL
Mitrofanov, Igor	Space Research Institute
Moersch, Jeff	University of Tennessee Knoxville
Mokrousov, Maxim	Space Research Institute
Molina Jurado, Antonio	CAB (Centro de Astrobiología)
Moores, John	York University
Mora-Sotomayor, Luis	CAB (Centro de Astrobiología)
Morookian, John Michael	NASA JPL
Morris, Richard	NASA JSC
Morrison, Shaunna	University of Arizona
Mueller-Mellin, Reinhold	University of Kiel
Muller, Jan-Peter	UCL (University College London)

Muñoz Caro, Guillermo	CAB (Centro de Astrobiología)
Nachon, Marion	LPGN (Laboratoire de Planétologie et Géodynamique de Nantes)
Navarro López, Sara	CAB (Centro de Astrobiología)
Navarro-González, Rafael	UNAM (University Nacional Autónoma de México)
Nealson, Kenneth	USC (University of Southern California)
Nefian, Ara	Carnegie Mellon University (at NASA Ames)
Nelson, Tony	LANL (Los Alamos National Lab)
Newcombe, Megan	Caltech
Newman, Claire	Ashima Research
Newsom, Horton	University of New Mexico
Nikiforov, Sergey	Space Research Institute
Niles, Paul	NASA JSC
Nixon, Brian	MSSS (Malin Space Science Systems)
Noe Dobrea, Eldar	PSI (Planetary Science Institute)
Nolan, Thomas	Nolan Engineering (at NASA GSFC)
Oehler, Dorothy	Jacobs Technology (at NASA JSC)
Ollila, Ann	University of New Mexico
Olson, Timothy	Salish Kootenai College
Owen, Tobias	University of Hawai'i at Manoa
Pablo Hernández, Miguel Ángel de	Universidad de Alcalá de Henares
Paillet, Alexis	CNES (Centre National d'Etudes Spatiales)
Pallier, Etienne	IRAP (Institut de Recherche en Astrophysique et Planetologie)
Palucis, Marisa	University of California Berkeley
Parker, Timothy	NASA JPL

Parot, Yann	IRAP (Institut de Recherche en Astrophysique et Planetologie)
Patel, Kiran	Global Science & Technology, Inc. (at NASA GSFC)
Paton, Mark	FMI (Finnish Meteorological Institute)
Paulsen, Gale	Honeybee Robotics
Pavlov, Alex	NASA GSFC
Pavri, Betina	NASA JPL
Peinado-González, Verónica	CAB (Centro de Astrobiología)
Pepin, Robert	University of Minnesota
Peret, Laurent	ATOS Origin
Perez, Rene	CNES (Centre National d'Etudes Spatiales)
Perrett, Glynis	University of Guelph
Peterson, Joe	SwRI (Southwest Research Institute)
Pilorget, Cedric	Caltech
Pinet, Patrick	IRAP (Institut de Recherche en Astrophysique et Planetologie)
Pla-García, Jorge	CAB (Centro de Astrobiología)
Plante, Ianik	USRA (at NASA JSC)
Poitrasson, Franck	CNRS (Centre National de la Recherche Scientifique) and GET (Géosciences Environnement Toulouse)
Polkko, Jouni	FMI (Finnish Meteorological Institute)
Popa, Radu	USC (University of Southern California)
Posiolova, Liliya	MSSS (Malin Space Science Systems)
Posner, Arik	NASA Headquarters
Pradler, Irina	University of Guelph
Prats, Benito	eINFORMe Inc. (at NASA GSFC)
Prokhorov, Vasily	Space Research Institute

Purdy, Sharon Wilson	Smithsonian Institution
Raaen, Eric	NASA GSFC
Radziemski, Leon	Piezo Energy Technologies, Tucson
Rafkin, Scot	SwRI (Southwest Research Institute)
Ramos, Miguel	Universidad de Alcalá de Henares
Rampe, Elizabeth	NASA Postdoc Program (at NASA JSC)
Raulin, François	LISA (Laboratoire Interuniversitaire des Systèmes Atmosphériques), Université Paris
Ravine, Michael	MSSS (Malin Space Science Systems)
Reitz, Günther	DLR (Deutsches Zentrum für Luft- und Raumfahrt)
Rennó, Nilton	University of Michigan Ann Arbor
Rice, Melissa	NASA Postdoc Program (at Caltech)
Richardson, Mark	Ashima Research
Robert, François	(LMCM) Laboratoire de Minéralogie et Cosmochimie du Muséum
Robertson, Kevin	Brown University
Rodriguez Manfredi, José Antonio	CAB (Centro de Astrobiología)
Romeral-Planelló, Julio J.	CAB (Centro de Astrobiología)
Rowland, Scott	University of Hawai'i at Manoa
Rubin, David	USGS Santa Cruz
Saccoccio, Muriel	CNES (Centre National d'Etudes Spatiales)
Salamon, Andrew	MSSS (Malin Space Science Systems)
Sandoval, Jennifer	MSSS (Malin Space Science Systems)
Sanin, Anton	Space Research Institute
Sans Fuentes, Sara Alejandra	CAB (Centro de Astrobiología)
Saper, Lee	MSSS (Malin Space Science Systems)

Sarrazin, Philippe	inXitu
Sautter, Violaine	LMCM (Laboratoire de Minéralogie et Cosmochimie du Muséum)
Savijärvi, Hannu	University of Helsinki
Schieber, Juergen	Indiana University Bloomington
Schmidt, Mariek	Brock University
Schmidt, Walter	FMI (Finnish Meteorological Institute)
Scholes, Daniel "Dan"	WUSTL (Washington University in St. Louis)
Schoppers, Marcel	NASA JPL
Schröder, Susanne	IRAP (Institut de Recherche en Astrophysique et Planetologie)
Schwenzer, Susanne	Open University
Sebastian Martinez, Eduardo	CAB (Centro de Astrobiología)
Sengstacken, Aaron	NASA JPL
Shterts, Ruslan	Space Research Institute
Siebach, Kirsten	Caltech
Siili, Tero	FMI (Finnish Meteorological Institute)
Simmonds, Jeff	NASA JPL
Sirven, Jean-Baptiste	CEA (Commissariat à l'Énergie Atomique et aux Énergies Alternatives)
Slavney, Susie	WUSTL (Washington University in St. Louis)
Sletten, Ronald	University of Washington Seattle
Smith, Michael	NASA GSFC
Sobrón Sánchez, Pablo	CSA (Canadian Space Agency)
Spanovich, Nicole	NASA JPL
Spray, John	University of New Brunswick
Squyres, Steven	Cornell University

Stack, Katie	Caltech
Stalport, Fabien	LISA (Laboratoire Interuniversitaire des Systèmes Atmosphériques)
Steele, Andrew	Geophysical Lab, Carnegie Institution of Washington
Stein, Thomas	WUSTL (Washington University in St. Louis)
Stern, Jennifer	NASA GSFC
Stewart, Noel	Salish Kootenai College
Stipp, Susan Louise Svane	University of Copenhagen
Stoiber, Kevin	MSSS (Malin Space Science Systems)
Stolper, Ed	Caltech
Sucharski, Bob	USGS Flagstaff
Sullivan, Rob	Cornell University
Summons, Roger	MIT
Sumner, Dawn	University of California Davis
Sun, Vivian	Brown University
Supulver, Kimberley	MSSS (Malin Space Science Systems)
Sutter, Brad	Jacobs Technology (at NASA JSC)
Szopa, Cyril	LATMOS (Laboratoire Atmosphères, Milieux, Observations Spatiales)
Tan, Florence	NASA GSFC
Tate, Christopher	University of Tennessee Knoxville
Teinturier, Samuel	LATMOS (Laboratoire Atmosphères, Milieux, Observations Spatiales)
ten Kate, Inge	Utrecht University
Thomas, Peter	Cornell University

Thompson, Lucy	University of New Brunswick
Tokar, Robert	Planetary Science Institute
Toplis, Mike	IRAP (Institut de Recherche en Astrophysique et Planetologie)
Torres Redondo, Josefina	CAB (Centro de Astrobiología)
Trainer, Melissa	NASA GSFC
Treiman, Allan	(LPI) Lunar and Planetary Institute
Tretyakov, Vladislav	Space Research Institute
Urqui-O'Callaghan, Roser	CAB (Centro de Astrobiología)
Van Beek, Jason	MSSS (Malin Space Science Systems)
Van Beek, Tessa	MSSS (Malin Space Science Systems)
VanBommel, Scott	University of Guelph
Vaniman, David	PSI (Planetary Science Institute)
Varenikov, Alexey	Space Research Institute
Vasavada, Ashwin	NASA JPL
Vasconcelos, Paulo	University of Queensland
Vicenzi, Edward	Smithsonian Institution
Vostrukhin, Andrey	Space Research Institute
Voytek, Mary	NASA Headquarters
Wadhwa, Meenakshi	ASU (Arizona State University)
Ward, Jennifer	WUSTL (Washington University in St. Louis)
Webster, Chris	NASA JPL
Weigle, Eddie	Big Head Endian LLC
Wellington, Danika	ASU (Arizona State University)
Westall, Frances	CNRS (Centre National de la Recherche Scientifique)

Wiens, Roger Craig	LANL (Los Alamos National Lab)
Wilhelm, Mary Beth	NASA Ames and Georgia Institute of Technology
Williams, Amy	University of California Davis
Williams, Joshua	University of New Mexico
Williams, Rebecca	PSI (Planetary Science Institute)
Williams, Richard B. "Mouser"	LANL (Los Alamos National Lab)
Wilson, Mike	UCSF (University of California San Francisco) (at NASA Ames)
Wimmer-Schweingruber, Robert	University of Kiel
Wolff, Mike	SSI (Space Science Institute)
Wong, Mike	University of Michigan Ann Arbor
Wray, James	MSSS (Malin Space Science Systems)
Wu, Megan	MSSS (Malin Space Science Systems)
Yana, Charles	CNES (Centre National d'Etudes Spatiales)
Yen, Albert	NASA JPL
Yingst, Aileen	PSI (Planetary Science Institute) (at University of Wisconsin)
Zeitlin, Cary	SwRI (Southwest Research Institute)
Zimdar, Robert	MSSS (Malin Space Science Systems)
Zorzano Mier, María-Paz	CAB (Centro de Astrobiología)